

History Effects in fatigue under variable amplitude loading mode I conditions in a 316L Stainless steel

F. Fremy¹ and S. Pommier¹ and E. Galenne²

¹LMT-Cachan (ENS Cachan/CNRS/Universite Paris 6/UniverSud Paris), 61 Avenue du Président Wilson 94235 Cachan, France. fremy@lmt.ens-cachan.fr pommier@lmt.ens-cachan.fr

²EDF R&D, Department Analysis in Mechanics and Acoustics, 1 avenue du Général de Gaulle 92141 Clamart, France. erwan.galenne@edf.fr

ABSTRACT. *Plastic deformation introduces internal stresses in the crack tip region that modify crack growth (direction and kinetics). Therefore, fatigue crack propagation models for metallic materials have to care about history effects. A model was developed for mode I fatigue crack growth under variable amplitude loading conditions. The purpose of this work is to extend it for a 316L steel which contained both isotropic and kinematic non-linear hardening. To identify the parameters of the model, a multiscale approach is used to transpose local results obtained using FE simulations of crack tip cyclic plastic deformation at the global scale. Several experiments were made using potential drop as a measurement of crack tip propagation and also Digital Image Correlation (DIC) which allows us field measurement. SEM fractographies were also performed to determine the fatigue crack growth rate at a local scale. The 316L steel displays cyclic hardening, which is then also found at the global scale. A direct consequence of this is an increase of the overload retardation effect with the number of consecutive overloads. This effect is found both using FE simulations and in the experiments, under mode I conditions.*

INTRODUCTION

Crack tip plasticity is known to be at the origin of spectacular memory effects in fatigue of metallic materials [1-8]. That makes difficult the modelling of fatigue crack growth under variable amplitude loads. These effects are related to the elastic-plastic behaviour of the material. The application of a mode I overload delays the fatigue crack growth. The overload yields the material ahead of the crack tip creating compressive residual stresses in the overload's plastic zone. As a consequence, the efficiency of subsequent fatigue cycles is reduced and the rate of fatigue crack growth is decreased. This is commonly known as plasticity-induced crack closure [1] effect. In addition, if the overload's ratio is large enough, the crack may grow under mixed-mode conditions until it has gone round the overload's plastic zone [2]. Thus, crack tip plasticity can modify both the kinetics and the crack's plane [2]. Therefore modelling the growth of a fatigue

crack under complex loading conditions requires a detailed analysis of the effects of crack tip plasticity.

Finite element methods are useful for analyzing crack tip plasticity under various loading conditions [3]. In particular, FE analyses allow accounting for rather complex material constitutive behaviour. However, the simulation of mode I or mixed-mode fatigue crack growth by elastic-plastic finite element computations leads to huge computation cost. In order to model service conditions in engineering applications, the computations became even more expensive because real components typically have fatigue lives of a few millions cycles, and cracks do not generally remain planar. The objective of the proposed methodology is to combine the precision of local finite element computations with the rapidity of a global approach [9].

For the sake of clarity, the principles of the technique will be briefly explained for elastic-plastic pure mode I cracks, then the developments that were added in order to take into account the effects of the 316L cyclic hardening law will be discussed.

EXPERIMENTS

For this experiment, we used CCT (*Center Cracked tension*) specimens, furnished by EDF. Their dimensions are 200*100*5mm. We performed two experiments: a constant amplitude fatigue crack growth test to get a reference fatigue crack growth law for the 316L stainless steel and a variable amplitude fatigue crack growth experiment, to evaluate history effects. For this purpose, 10 overloads were applied every 9990 constant amplitude fatigue cycles; the overload ratio was fixed at 1.34.

It is observed that the application of periodic overloads increases very significantly the fatigue life. A retardation effect of about a factor 3 is found in this case.

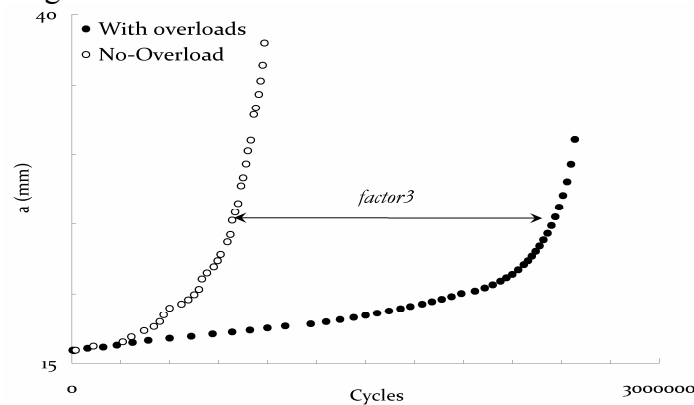


Figure 1. Evolution of the crack length measured with or without overloads in a 316L stainless steel.

The fracture surface was observed using a scanning electron microscope for a stress intensity factor around $20 \text{ MPa}\cdot\text{m}^{1/2}$ in both cases. When constant amplitude fatigue cycles are used, the crack growth is planar, and fatigue striations are clearly visible (Fig. 2a) [10]. The striations spacing is around 200nm.

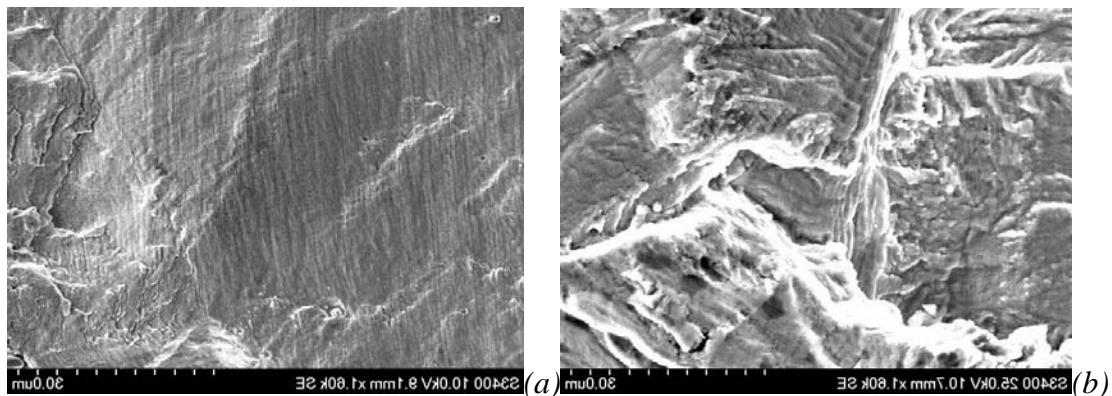


Figure 2. SEM images taken for $DK=20\text{MPa}\cdot\text{m}^{1/2}$ (a) for a constant amplitude fatigue test (b) for a variable amplitude fatigue test.

On the contrary, the fracture surface is rough when variable amplitude fatigue is used (Fig. 2b). Periodic markings can be seen on the fracture surface (Fig. 3a), which correspond to the traces of crack tip blunting during each block of 10 overloads cycles. As a consequence, the distance between 2 markings is equal to the crack propagation during 10 000 loading cycles, which allows evaluating the average crack growth rate directly from fractographic observations. It can be observed that this average crack growth rate is of 70 nm per cycle. The average crack growth rate determined from fractographies is therefore about three times smaller when overloads are applied compared with constant amplitude fatigue.

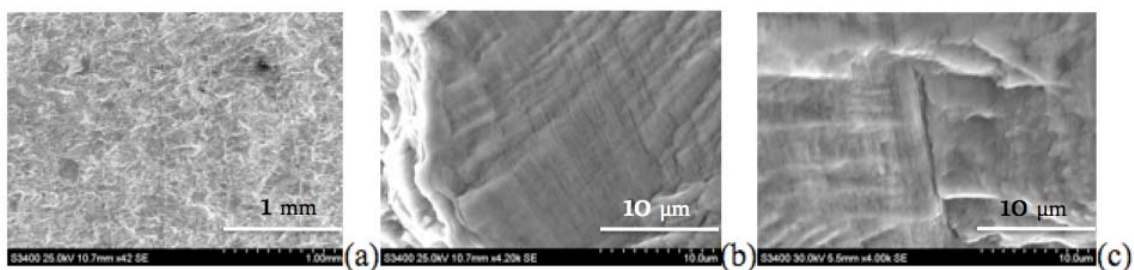


Figure 3. SEM images taken for $DK=20\text{MPa}\cdot\text{m}^{1/2}$ for the variable amplitude fatigue test.(a) global view with markings when 10 overloads are applied every 10000 cycles.

(b) striation spacing just after the application of the overloads.(d) secondary cracks observed at a distance of about 50 μm from the marking left by the overload.

Using SEM images it was possible to observe also the local crack propagation rate. The 10 overloads leave large striations on the fracture surface (Fig. 3a) and the crack blunts significantly (by more than 5 micrometers). Just after the overloads block, very clear striations can be observed, with a striation spacing of about 400 nm (Fig. 3b) which indicates an increase of the crack growth rate just after the application of the overload, by about a factor two by comparison with that observed in constant amplitude fatigue. Then at about 50 micrometers from the last marking left by an overload block, the fracture surface becomes rough and secondary cracks can be observed (Fig. 3c)

which indicates a significant reduction of the local crack growth rate along the mode I crack growth plane. As a consequence, if less than a hundred of constant amplitude cycles are applied between each block of 10 overloads, a very significant increase of the average fatigue crack growth rate should be observed by comparison with a constant amplitude fatigue test.

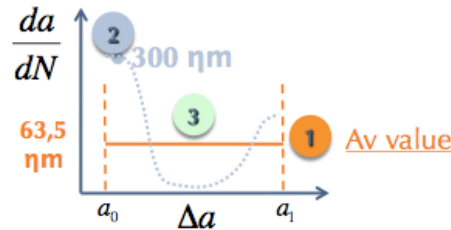


Figure 4. Evolution of the crack growth rate between 2 blocks of 10 overloads (1) Average value of the crack growth rate between 2 blocks of 10 overloads and 9990 loads (2) local measurement on the crack surface with SEM, (3) observations of secondary cracks, meaning strong reductions of crack growth rate.

It is therefore important to recognize that this problem cannot be modelled by a unique mechanism, such as the increase of the crack opening level when the crack tip propagates inside the overloads plastic zone. At least three phenomena are observed here, a large crack tip blunting during the application of the overloads, a transient but significant increase of the crack growth rate after the overloads, and finally a drop off of the crack growth rate. Therefore history effects in this material may introduce complex dependencies to the distribution of peaks in a load spectrum, which are aimed at being modelled in the future.

MATERIAL CONSTITUTIVE MODEL

The FE method is used to compute the details of the evolution of plastic deformation, residual stresses, stress range etc... within and around the crack tip region for a stationary or a moving crack tip. The main advantage of using the FE method is that it allows using complex material constitutive behaviours, which is usually needed for engineering alloys. For this purpose, we need first to identify a cyclic elastic-plastic constitutive law for the 316L stainless steel.

The identification procedure of the parameters in the model f requires the knowledge of the material cyclic elastic-plastic behaviour. It is performed using the FE method and is fully automatic and cheap in computation cost. In order to characterize the elastic-plastic constitutive behaviour of the 316L steel, we used a cylindrical specimen, with a diameter of 16mm thick. Strain controlled push-pull tests were performed with increasing strain amplitude (Fig. 5). The material displays both kinematic and isotropic hardening. Therefore, at each level, we performed 30 cycles so as to characterize the isotropic hardening of the material. The cyclic elastic-plastic

behaviour of this material was modelled using the Von Mises yield criterion and the coupled non-linear hardening law, standard in Abaqus 6.5 and detailed in Eq. 1 to 4.

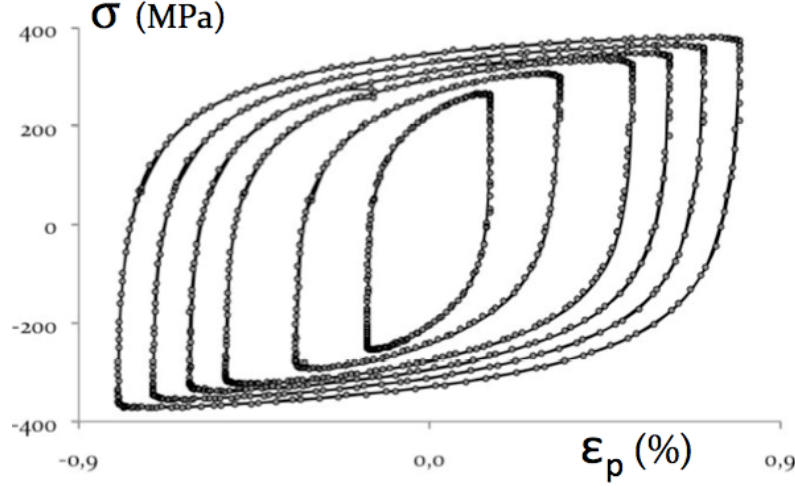


Figure 5. strain-controlled push pull test in the 316L stainless steel – Stress (MPa) versus plastic strain (%). 30 cycles are applied at each level of the strain amplitude.

The 7 material parameters used for the simulations are reported in Table 1. A reasonable agreement is found between experiments and simulations (Fig. 6).

$$\underline{\underline{\sigma}} = \lambda \text{Tr} \underline{\underline{\varepsilon}} \underline{\underline{I}} + 2\mu \underline{\underline{\varepsilon}} \quad \text{Isotropic Elasticity} \quad (1)$$

$$f = \sqrt{\frac{3}{2} (\underline{\underline{\sigma}}' - \underline{\underline{X}}) : (\underline{\underline{\sigma}}' - \underline{\underline{X}})} - R \quad \text{Von Mises yield criterion} \quad (2)$$

$$\underline{\underline{\sigma}}' = \underline{\underline{\sigma}} - \frac{\text{Tr} \underline{\underline{\sigma}}}{3} \underline{\underline{I}} \quad \text{Consistency } \dot{Y} = 0 \quad (3)$$

$$\underline{\underline{\dot{\alpha}}}_p = \dot{\lambda} \frac{\partial f}{\partial \underline{\underline{\sigma}}} \quad \text{Normal flow law} \quad (4)$$

$$R = R_0 + Q \times (1 - e^{-bp}) \quad \text{Isotropic hardening law} \quad (5)$$

$$\dot{\lambda} = \sqrt{\frac{2}{3} \underline{\underline{\dot{\alpha}}}_p : \underline{\underline{\dot{\alpha}}}_p} \quad \text{Comportement élastique} \quad (6)$$

$$\underline{\underline{X}} = C \underline{\underline{\dot{\alpha}}}_p - \gamma \underline{\underline{X}} \dot{\lambda} \quad \text{Kinematic hardening law} \quad (7)$$

Parameters $\{\lambda, \mu, R_0, Q, b, C, \gamma\}$

These parameters were used to simulate the push-pull test and to quantify the adjustment error. Then this constitutive behaviour is used for the finite element simulations of the cyclic behaviour of an elastic-plastic centre cracked FE model under variable amplitude mode I loading conditions.

E (GPa)	ν	R_0 (MPa)	Q (MPa)	γ	C	b
187	0,3	110	90	580	112500	0,3

Table 1 Parameters of the elastic-plastic constitutive law used in the model

MULTISCALE APPROACH

A multiscale approach is used to transpose at the global scale the local results obtained using FE simulations of crack tip cyclic plastic deformation. Next, the set of curves generated by post-treating FE computations using that multiscale approach are used to identify an empirical global cyclic elastic-plastic constitutive law (denoted by f) for the crack tip region with a global point of view. In this case, we used this method model in pure mode I conditions. A general elastic-plastic law is assumed for the material behaviour in the crack tip region. Thus, the displacement field in the crack tip region can be partitioned into as a sum of two components, an “elastic” and a “plastic” component. In addition, each of these components is defined as the product of an intensity factor and a reference field. The reference fields are determined first, using preliminary FE computations which the “elastic” reference field $\underline{u}_I^e(\underline{x})$ is the solution, using boundary conditions such as that $K_{I1}=1 \text{ MPa}\cdot\text{m}^{1/2}$. Then a monotonic mode I loading ramp is simulated using this time the elastic-plastic behaviour of the material. At the end of the computation, the intensity $\tilde{K}_I(t)$ of the “elastic” part is determined as the projection of the computed displacement field $\underline{u}(\underline{x},t)$ onto $\underline{u}_I^e(\underline{x})$:

$$\tilde{K}_I(t) = \frac{\int \underline{u}(\underline{x},t) \cdot \underline{u}_I^e(\underline{x})}{\int \underline{u}_I^e(\underline{x}) \cdot \underline{u}_I^e(\underline{x})} \quad (8)$$

The rest of the displacement field is then calculated so as to define the “plastic” reference field, $\underline{u}_I^c(\underline{x})$ orthogonal by construction to $\underline{u}_I^e(\underline{x})$: $\int \underline{u}_I^c(\underline{x}) \cdot \underline{u}_I^e(\underline{x}) = 0$.

$$\underline{u}_I^c(\underline{x}) = B(\underline{u}(\underline{x},t) - \tilde{K}_I(t)\underline{u}_I^e(\underline{x})) \quad (9)$$

The coefficient B is adjusted so that the average value of the discontinuity of $\underline{u}_I^c(\underline{x})$ is equal to $1\mu\text{m}$ along the crack faces within a distance to the crack tip of one tenth of the crack length. The two orthogonal reference fields are used in the following as a basis to project (eq. 8, eq. 10) the displacement field within the crack tip region during each time increment of various variable amplitude loading schemes:

$$\rho_I(t) = \frac{\int \underline{u}(\underline{x},t) \cdot \underline{u}_I^c(\underline{x})}{\int \underline{u}_I^c(\underline{x}) \cdot \underline{u}_I^c(\underline{x})} \quad (10)$$

Then, so as to identify the model, various elastic plastic FE computations are performed to generate evolutions of $\rho_I(t)$. So as to build a variational approach, only small time increments are considered. The displacement field $d\underline{u}(\underline{x},t)$ during each time increment is approached according to Eq. 11 : $d\underline{u}(\underline{x},t) \approx d\tilde{K}_I(t)\underline{u}_I^e(\underline{x}) + d\rho_I(t)\underline{u}_I^c(\underline{x})$ (11)

The error $C(t)$ associated with this approximation (Eq. 12) is also calculated and remains usually well below 10%.

$$C(t) = \sqrt{\frac{\int \left[d\underline{u}(\underline{x},t) - \left[d\tilde{K}_I(t)\underline{u}_I^e(\underline{x}) + d\rho_I(t)\underline{u}_I^c(\underline{x}) \right] \right]^2}{\int d\underline{u}(\underline{x},t)^2}} \quad (12)$$

This method enables to characterize the cyclic elastic-plastic displacement field in the crack tip region at the global scale, through two intensity factors only, $\tilde{K}_I(t)$, which is close to the nominal stress intensity factor $K_I^\infty(t)$, and $\rho_I(t)$, which measures crack tip plasticity at the global scale. The advantage of this methodology is that it can be applied to any material constitutive law. In practice, the approximation in Equation 8 is performed at each step of a finite element computation using a post-treatment routine.

This model can be all summed up into a set of about ten scalar partial differential equations. It provides the global plasticity rate $d\rho_I/dt$ within the crack tip region as a function of the nominal loading rate dK_I^∞/dt and of the current state of a set of internal variables $(\phi_c, \phi_{Xc}, \phi_m, \phi_{Xm})$. To finalize the model, a crack growth law is also introduced. It states that the rate of production of cracked area per unit of the crack front da/dt is proportional to the global plasticity rate $|d\rho_I/dt|$. This hypothesis derives merely from the well-known Δ CTOD equation. Then, once identified, the global model can be used to predict the fatigue crack growth rate for variable amplitude loadings schemes. It accounts for plasticity induced history effects and is cheap in computation cost.

a_m	b_m	a_{cf}	b_{cf}	a_{xm}	p_a	k_a	k_b
14,1	2,0	20,9	5,1	-1,4	$-6,0 \cdot 10^{-4}$	$-6,1 \cdot 10^{-2}$	$-5,1 \cdot 10^{-2}$

Table 2 Parameters of the evolutions law of the model (See. [11])

RESULTS

We performed 4 different experiments and the simulations related to them. The goal is to compare the results obtained by the analytic solution furnished by our model (represented by continuous lines) and the crack growth rates measured experimentally (represented by discrete points).

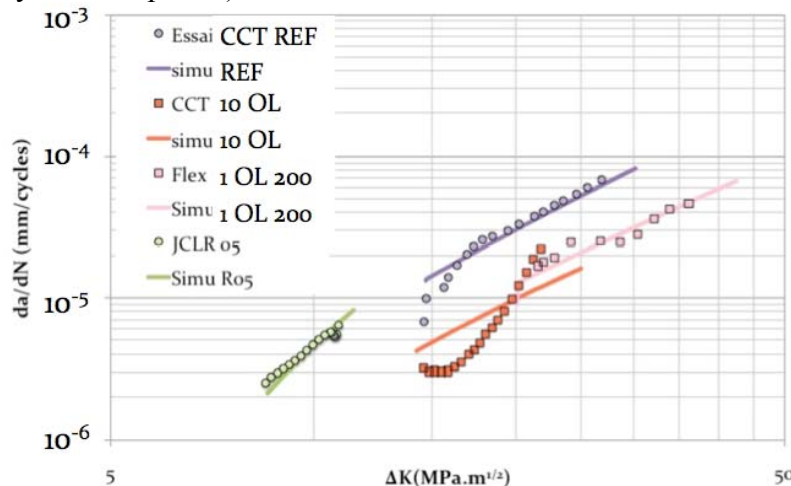


Figure 6. Experiments and simulations performed for 4 types of loadings (ModeI). REF - without overload and R-ratio = 0,1 / JCLR - without overload and R-ratio = 0,5 / 10OL - 10 overloads every 9990 loads / 1OL200 - one overload every 200 loads.

We performed an experiment without any overload and a R-ratio of 0.1 (REF), then another experiment by EDF without any overload but with a R-ratio of 0.5 (JCLR). Two experiments with overloads were accomplished: one with an overload every 200 loads (1OL200) and another one with a block of 10 overloads every 9990 loads (10OL). The level of the overload ratio is 1.34 for both experiments. The agreement between the model and the experimental results is very good for the 3 first experiments. The strong non-linearity that we observed for the last experiment highlights the difficulty to modelise those phenomena. The calculation of the propagation of the crack takes about 2 minutes, this is an advantage of this modelisation and an objective for an engineering utilisation. For more details about the methodology to identify the model, see [11].

CONCLUSION

The 316L steel displays non-linear cyclic hardening, which is also found at the global scale. A direct consequence of this is an increase of the overload retardation effect with the number of consecutive overloads. This effect is found both using FE simulations and in the experiments, under mode I variable loading amplitude conditions. The goal of this work is to understand and to model the complex hardening of this material and introduce it in our approach. The multiscale approach used save time and expensive FE simulations since the simulations of the propagation of a crack are very fast.

The results that we obtained showed good consistency with the experiments that we performed although we still need to work to understand better the block effect of overloads. Our approach developed for mode I conditions will be extended for mixed mode conditions under mode I+II+III with overloads.

REFERENCES

1. W. Elber, ASTM STP 486, 1971, pp. 230-242.
2. S. Suresh, *Fatigue of Materials*, Cambridge University Press, Cambridge, 1991.
3. Mc Clung. proc. Fatigue 96, 6th International Fatigue Congress, Berlin FRG, 6-10 May 1996.
4. J. Lemaitre et J.L. Chaboche, *Mécanique des matériaux solides*, Dunod, Paris, 1985, 213-234
5. Pommier, S., Lopez-Crespo, P., Decreuse P.Y. *Fatigue & Fracture of Engineering Materials & Structures*. Vol 32. Pages 899-915. 2009R.C.
6. N.A. Fleck and J.C Newman. *ASTM STP 982*, 1988, pp. 319-341
7. J.C. Newman. *ASTM STP 748*, 1981, pp. 53-84
8. J. Schijve. *Engineering Fracture Mechanics*, (5) 1973, pp. 269-280, 1973.
9. Pommier, S., Hamam, R. *Fatigue & Fracture of Engineering Materials & Structures*. Vol 30. Num 7. Pages 582-598. 2007
10. J.C McMillan and R.M.N Pelloux. *ASTM STP 415*, 1967, pp. 505-532, 1967